Harmonic Debye-Waller analysis of anharmonic vibrations

D. J. Safarik, A. Llobet, and J. C. Lashley
Los Alamos National Laboratory, Los Alamos, New Mexico 87545, USA
(Received 10 February 2012; published 11 May 2012)

We address the error resulting from application of the harmonic Debye-Waller factor to anharmonic vibrations. The mean-square atomic displacement $\langle u^2 \rangle$ determined from the harmonic analysis is compared to values obtained from an exact anharmonic analysis. In the case of strong anharmonicity, we find that the harmonic approximation introduces at most a ∼25% error. The temperature dependence determined from the harmonic analysis follows that found from the exact anharmonic analysis. Errors introduced by the harmonic approximation are comparable in magnitude to the usual systematic errors associated with diffraction experiments and Rietveld refinements.

DOI: 10.1103/PhysRevB.85.174105 PACS number(s): 61.05.fm, 63.20.Ry, 63.70.+h

I. INTRODUCTION

Static or dynamic lattice disorder causes a decrease in the intensity of the Bragg diffraction peaks. This decrease results from partial decoherence of the scattered photons, neutrons, or electrons.[1] The reduced Bragg intensities, after the usual corrections for absorption, Lorenz-polarization, etc., are normally interpreted in terms of a Debye-Waller factor. Debye-Waller factors account for the effect of lattice disorder on the overall intensity of a particular Bragg reflection. These factors quantify the intensity reduction due to the atomic mean-square displacements from equilibrium.[2]

In the refinement of diffraction data using the general structure analysis system (GSAS)[3] or other Rietveld packages, connections between diffracted intensity and the mean-square atomic displacements (MSADs) are usually made via the standard expression for the temperature factor T_j. For isotropic atomic displacements, this expression is $T_j = \exp(-8\pi^2 \langle u^2_{\mathrm{iso},j} \rangle \sin^2\theta/\lambda^2)$, where $\langle u^2_{\mathrm{iso},j} \rangle$ is the isotropic mean-square displacement of the atom in Wyckoff site j, θ is the Bragg angle, and λ is the wavelength.[2,3] For anisotropic displacements, the temperature factor becomes $T_j = \exp(-2\pi^2[\langle u^2_{1,j} \rangle h^2 b_1^2 + \cdots + 2\langle u_{1,j} u_{2,j} \rangle hkb_1b_2 + \cdots])$. Here, h, k, and l are Miller indices; b_1, b_2, and b_3 are the Cartesian components of the reciprocal lattice vectors; and $\langle u^2_{1,j} \rangle$, $\langle u_{1,j} u_{2,j} \rangle$, etc. are the mean-square anisotropic displacements.[2,3] These equations are of course derived strictly for the case of a harmonic oscillator.[2] We therefore expect the values of $\langle u^2_j \rangle$ deduced from the refinement to be accurate only for atoms that vibrate harmonically, or nearly so. For most materials and conditions, the phonons have only mild anharmonicity, so the restriction of T_j to harmonic vibrations is not a serious limitation.

Since the 1990s, there has been growing interest in strongly anharmonic vibrations and the physics associated with them. By *strong* anharmonicity we mean that the anharmonicity cannot be considered simply as a perturbation of the harmonic model. Much of this interest has been motivated by rattling-mode crystals such as clathrates and filled skutterudites. The structures of these materials are characterized by networks of polyhedral cages that are capable of accommodating guest atoms or molecules.[4–8] If the cage is oversized compared to the guest, then the guest can vibrate with low frequency, large amplitude, and often times with strong anharmonicity.[4–12] Guest atom rattling is associated with several interesting physical phenomena, including superconductivity,[13,14] heavy fermion behavior,[15,16] and strong scattering of heat-carrying acoustic phonons.[4–8] The latter phenomenon is being exploited to develop new thermoelectric materials with enhanced figures of merit.[17,18]

Anharmonic vibrations are also encountered in the vicinity of phase transitions, for example, ferroelectric,[19–21] martensitic,[22] and distortive transformations.[23] These diffusionless transitions are associated with the softening of particular optical-phonon branches.[19–24] In this case, the anharmonicity evidently corresponds to fluctuations in the atomic positions at certain crystallographic sites.[25] Near the transition, the atomic fluctuations are coupled by long-range elastic interactions resulting in the collective motion that characterizes the transformation. This is different from rattling-mode materials, where the vibrations appear to be more localized.[4–6,9–12]

To treat anharmonic vibrations in a rigorously correct manner, we must refine the diffraction data using an anharmonic model for the Debye-Waller factor. In principle, this is the only way to obtain accurate $\langle u^2_j \rangle$ values. Numerous models for the anharmonic Debye-Waller factor have appeared in the literature since the 1960s.[26–35] These models are based mainly on statistical methods[26–29,36] or on single-particle models of the anharmonic potential.[29–35] Statistical approaches[26–29] calculate T_j from the probability distribution function for the atomic displacements. For a harmonic vibration, the atomic displacements follow a Gaussian distribution, so simple statistical analyses give the harmonic T_j.[36] For an anharmonic vibration, the probability distribution function is not Gaussian. In this case, non-Gaussian statistical formalisms are used to calculate the anharmonic T_j.[26–29] The two formulations used most frequently are the Edgeworth expansion and the Gram-Charlier expansion.[27,36] Both have the general form $T_j = T_{j,h}[a_3 + a_4 + \cdots]$, where $T_{j,h}$ is the harmonic (Gaussian) temperature factor and a_3,a_4, etc. are higher-order cumulants of the distribution that are associated with the third-, fourth-, etc. order anharmonic terms of the potential. For an anisotropic vibration, there are 10 coefficients associated with the cubic cumulant, 15 associated with the quartic cumulant, etc. These coefficients are fitting parameters to be determined from the Rietveld refinement.

In single-particle potential models,[29–36] the interatomic potential is usually assumed to have the form $V(u) =$

$V_0 + \beta_{jk}u_ju_k + \gamma_{jkl}u_ju_ku_l + \delta_{jklm}u_ju_ku_lu_m + \cdots$. Here the second term on the right is the harmonic contribution and the following terms are the cubic, quartic, etc. anharmonic contributions. The allowable terms are dictated by the site symmetry. Anharmonic T_j are calculated from $V(u)$ using statistical mechanics, usually for the classical limit. The coefficients of the potential terms β_{jk}, γ_{jkl}, δ_{jklm}, etc. are fitting parameters determined from the refinement. We should note that the single-particle potential methods have a physical basis, whereas the statistical approaches are based simply on mathematical expansions.

There are several difficulties associated with the anharmonic analyses discussed above. First, commonly used Rietveld refinement packages such as GSAS[3] usually do not include anharmonic models for the Debye-Waller factor. Therefore one must develop custom Rietveld software that includes the relevant anharmonic models. No doubt this has already been done by diffraction experts, but such software is generally not available or intended for widespread use by the physics or materials science communities. Second, an anharmonic analysis adds a large number of fitting parameters to the Rietveld refinement. One must use care to ensure that the quality of the diffraction data justifies these extra parameters. Specifically, one must differentiate between those parameters that are physically meaningful and those that merely improve the fit to poor-quality data.[36]

In view of these difficulties, we would prefer to avoid the full anharmonic analysis. One approach is simply to ignore the anharmonicity and use the harmonic Debye-Waller factor. Maradudin and Flinn's[30] single-particle potential work from the early 1960s suggests that this may be a reasonable approximation. They found that for a cubic lattice with cubic and quartic anharmonicity, the Debye-Waller factor can be written as $T^2 = \exp(-2M)\exp(-2M_3 - 2M_4)$, where $\exp(-2M)$ is the usual harmonic contribution and $\exp(-2M_3 - 2M_4)$ are additional contributions arising from the cubic and quartic terms. Using the available literature data, Maradudin and Flinn evaluated these expressions for Pb. They found that even for temperatures near the melting point, including the anharmonic terms modifies the value of T^2 by $\sim$10% compared to using only the harmonic term. Dash *et al.*[32] later used single-particle models to address the case of *strong* anharmonicity, where the anharmonicity cannot be considered as a perturbation. This case seems more applicable to the anharmonic vibrations associated with rattling modes and soft-mode phase transitions. It was shown[32] that the anharmonic Debye-Waller factor could be expressed approximately as the product of harmonic and anharmonic contributions, similar to that found by Maradudin and Flinn. However, in contrast to Maradudin and Flinn's results for mild anharmonicity, Dash *et al.* found that for strong anharmonicity the anharmonic terms are not negligible.

In the present work, we explore using the *harmonic* Debye-Waller factor to analyze anharmonic vibrations, particularly those with strong anharmonicity. Specifically we assess the error in the values and temperature dependence of $\langle u_j^2\rangle$ associated with applying the harmonic model to anharmonic vibrations. The remainder of this paper is organized into four sections. In Sec. II, we define the temperature factor T_j and derive the form that is applicable to anharmonic vibrations. In Sec. III, we discuss our methods for determining the harmonic and anharmonic values of $\langle u_j^2\rangle$. In Sec. IV, we show that strongly anharmonic *rattling-mode* vibrations can indeed be analyzed in terms of the harmonic model, with relatively small errors in the magnitude and temperature dependence of $\langle u_j^2\rangle$. In Sec. V, we repeat this analysis for fluctuations in the vicinity of soft-mode phase transitions. We again find that the harmonic model gives satisfactory results, regardless of the anharmonicity of the vibration. Lastly, in Sec. VI, we compare our results to available experimental data.

II. THE TEMPERATURE FACTOR AND DEBYE-WALLER FACTOR

The intensity of a particular Bragg reflection is $I(hkl) \propto F^*(hkl) \times F(hkl)$, where

$$F(hkl) = \sum_j f_j T_j \exp[-i\,\vec{Q}(hkl)\cdot\vec{r}_j] = T\sum_j f_j \exp[-i\,\vec{Q}(hkl)\cdot\vec{r}_j], \quad (1)$$

is the structure factor and $F^*(hkl)$ is its complex conjugate.[2] In Eq. (1), f_j is the scattering strength of the atom in Wyckoff site j (as given by the atomic form factor or coherent neutron-scattering amplitude), $\vec{Q}(hkl)$ is the scattering wave vector, $\vec{r}_j$ is the equilibrium atomic position, T_j is the temperature factor for the atom in site j, and T is the effective temperature factor for the (hkl) reflection.[2] The Debye-Waller factor is T^2. The Debye-Waller factor accounts for the effect of lattice disorder on the overall intensity of the reflection. If all crystallographic sites have the same temperature factor, then the Debye-Waller factor is simply $T^2 = T_j^2$. If the sites have different T_j's, then T^2 can be a complicated function of T_j's and f_j's.

The temperature factor T_j appears naturally in Eq. (1) as a result of ensemble averaging over the instantaneous fluctuations of the atomic positions.[2,37,38] Expressed in its most fundamental form, the temperature factor is $T_j = \langle\exp[-i\,\vec{Q}(hkl)\cdot\vec{u}_j]\rangle$, where $\vec{u}_j$ is the instantaneous displacement from equilibrium due to all normal vibrational modes, and $\langle\cdot\rangle$ denotes the ensemble average over all atoms occupying site j. For a harmonic vibration, this general expression for T_j simplifies to the equations in the introduction.[2] This is easily verified using Bloch's identity.[2,39]

For an anharmonic vibration, Bloch's identity does not apply, and so the harmonic equations for T_j are not valid. In this case, we expand the exponential as a power series and ensemble average each term to obtain

$$T_j = 1 - i\langle\vec{Q}\cdot\vec{u}_j\rangle - \tfrac{1}{2}\langle(\vec{Q}\cdot\vec{u}_j)^2\rangle + \tfrac{1}{6}i\langle(\vec{Q}\cdot\vec{u}_j)^3\rangle + \tfrac{1}{24}\langle(\vec{Q}\cdot\vec{u}_j)^4\rangle - \tfrac{1}{120}i\langle(\vec{Q}\cdot\vec{u}_j)^5\rangle - \tfrac{1}{720}\langle(\vec{Q}\cdot\vec{u}_j)^6\rangle + \cdots. \quad (2)$$

Here we have dropped the (hkl) argument of $\vec{Q}$. Equation (2) is rigorously correct for any vibration, regardless of anharmonicity, provided that enough terms are evaluated to reach convergence. Depending on the magnitudes of $\vec{u}_j$ and $\vec{Q}$, tenth- or higher-order terms may be required.

III. METHODS

Our goal is to quantify the error in $\langle u_j^2 \rangle$ caused by using the harmonic temperature factor to analyze lattice vibrations with strong anharmonicity. One approach is to use actual diffraction data, such as for clathrates[4] or skutterudites,[18] and to refine the rattling atom site using both the harmonic model as well as various anharmonic models. The difference in the values of $\langle u_j^2 \rangle$ deduced from the harmonic and anharmonic models then gives the error. Most likely, this approach would not give an accurate estimate of the error because (i) one cannot be sure which, if any, of the assumed anharmonic models is correct, and (ii) systematic errors in the experiment and data analysis may be difficult or impossible to quantify.

In view of these limitations, here we will *model* various anharmonic vibrations using one-dimensional single-particle potentials. For each potential, we calculate the *anharmonic* mean-square displacement $\langle u_j^2 \rangle_A$ using quantum statistical mechanics. To do this, we solve the Schrödinger equation numerically for the assumed anharmonic potential, thus obtaining eigenenergies E_n and wave functions Ψ_n for the eigenstates n. We then compute the anharmonic mean-square atomic displacement (MSAD) from $\langle u_j^2 \rangle_A = \sum_n p_n \langle \Psi_n | u_j^2 | \Psi_n \rangle$, where $p_n = e^{-\beta E_n}/Z$ is the Boltzmann weight, $Z = \sum_n e^{-\beta E_n}$ is the partition function, $\beta = 1/k_B T$, and k_B is the Boltzmann constant. Our assumption of a one-dimensional interatomic potential means that a single value of $\langle u_j^2 \rangle_A$ characterizes the displacement. This is analogous to a cubic-symmetry crystallographic site, where the MSAD are isotropic and are characterized by one value of $\langle u_{\mathrm{iso},j}^2 \rangle$.[2]

To determine the *quasi-harmonic* mean-square displacement $\langle u_j^2 \rangle_{QH}$, we first calculate as a function of $|\vec{Q}(hkl)|^2 = 16\pi^2 \sin^2\theta/\lambda^2$ the reduction in Bragg intensities associated with a particle vibrating in the assumed anharmonic potential. This reduction of intensity is equal to the square of the anharmonic temperature factor T_j^2, as calculated by evaluating Eq. (2) to convergence. To evaluate the terms in Eq. (2), we must make an assumption about the symmetry of the crystal. For simplicity, and for consistency with our calculations of $\langle u_j^2 \rangle_A$, we assume a cubic crystal with all cubic-symmetry sites so that the MSAD are isotropic.[2] To evaluate the series, we must also compute the higher-order mean displacements $\langle u_j^m \rangle = \sum_n p_n \langle \Psi_n | u_j^m | \Psi_n \rangle$, where $m = 3,4,5 \ldots$. This is done numerically as described above for $\langle u_j^2 \rangle_A$.

After calculating these Bragg intensity "data" for our model anharmonic crystal, we analyze them using the harmonic and isotropic Debye-Waller factor, $T^2 = T_j^2 = \exp(-16\pi^2 \langle u_{\mathrm{iso},j}^2 \rangle_{QH} \sin^2\theta/\lambda^2)$. For this, we construct Wilson plots, Log I versus $\sin^2\theta/\lambda^2$, where I is the diffracted intensity. Here we assume that $I \propto T^2$. From the slopes of the Wilson plots, we then determine the quasiharmonic values $\langle u_{\mathrm{iso},j}^2 \rangle_{QH}$.

In calculating the Bragg intensities, we assumed that our crystal has only one type of cubic-symmetry site. In this case, the Debye-Waller factor is simply $T^2 = T_j^2$. By assuming that the site potential is strongly anharmonic, our model crystal represents an extreme (and perhaps unrealistic) case where *every* atom vibrates with strong anharmonicity. In contrast, for real crystals the anharmonic soft or rattling modes are usually confined to one type of lattice site, whereas the other sites are characterized by smaller anharmonicity. The point is that in our model crystal, the anharmonic atom contributes *all* of the the intensity to *every* (hkl) Bragg reflection, whereas for real crystals the anharmonic atom contributes differently to the intensities of the various Bragg reflections. As a result, the effect of anharmonicity on the peak intensities will probably be more pronounced in our fictitious crystal than in a real one.

TABLE I. One-dimensional single-particle potentials. θ_E is the characteristic vibrational temperature, m_e is the effective particle mass, u is the displacement from the well center (see insets of Fig. 1), and k_B and $\hbar$ are the Boltzmann and Planck constants, respectively. For the Morse potential, γ characterizes the well depth, whereas for the double well, α characterizes the height of the barrier separating the two minima. For the 2–4 Landau potential, T_c is the phase-transition temperature and a' describes the strength of the harmonic term.

Potential	$V(u)$
Harmonic	$\frac{1}{2}\left(\frac{k_B\theta_E m_e}{\hbar^2}\right)k_B\theta_E u^2$
Morse	$\gamma k_B\theta_E\left\{1-\exp\left[\left(\frac{k_B\theta_E m_e}{\hbar^2}\right)^{1/2}\frac{1}{\sqrt{2\gamma}}u\right]\right\}$
Sextic	$\frac{1}{6}\left(\frac{k_B\theta_E m_e}{\hbar^2}\right)^3 k_B\theta_E u^6$
2–4 Double well	$-\frac{\alpha}{2}\left(\frac{k_B\theta_E m_e}{\hbar^2}\right)k_B\theta_E u^2+\frac{1}{4}\left(\frac{k_B\theta_E m_e}{\hbar^2}\right)^2 k_B\theta_E u^4$
2–4 Landau	$\frac{1}{2}a'\frac{T-T_c}{\theta_E}\left(\frac{k_B\theta_E m_e}{\hbar^2}\right)k_B\theta_E u^2+\frac{1}{4}\left(\frac{k_B\theta_E m_e}{\hbar^2}\right)^2 k_B\theta_E u^4$

Modern structural refinements are usually performed via Rietveld-type whole-pattern methods, where $\langle u_{\mathrm{iso},j}^2 \rangle_{QH}$ values are extracted using a nonlinear least-squares fitting algorithm. For complicated crystal structures containing different types of sites, this is the only practical way to deduce MSAD values. For structures containing only one type of site, one may also use the Wilson plot analysis, as done here. In principle, the two methods should give the same values of $\langle u_{\mathrm{iso},j}^2 \rangle$. In practice, the linear Wilson analysis might be more reliable. The reason is that nonlinear algorithms such as those used in Rietveld refinements are known to get stuck near boundaries of the parameter space, or get lost in regions of parameter space where the model is unresponsive to changes in the parameter values.[40]

We performed this analysis for the five single-particle potentials listed in Table I: harmonic, Morse, sextic (sixth-order), 2–4 double-well, and 2–4 Landau. The harmonic potential was chosen as a check on the self-consistency of our methods. The Morse potential was chosen because it captures qualitatively the "high-temperature" anharmonicity exhibited by most solids (although this particular potential is more often used to describe covalent bonding in molecules). Sextic and 2–4 double-well potentials model the anharmonic "rattling modes" found in certain clathrates,[4] filled skutterudites,[17] β-pyrochlore oxides,[11] and VAl_{10}.[41] Finally, the 2–4 Landau potential approximates optical vibrations in the vicinity of soft-mode phase transitions. For each potential, the above-described calculations were done for various effective particle masses m_e and characteristic vibrational temperatures θ_E, as characterized by the quantity $\hbar^2/(m_e k_B \theta_E)$. Calculations

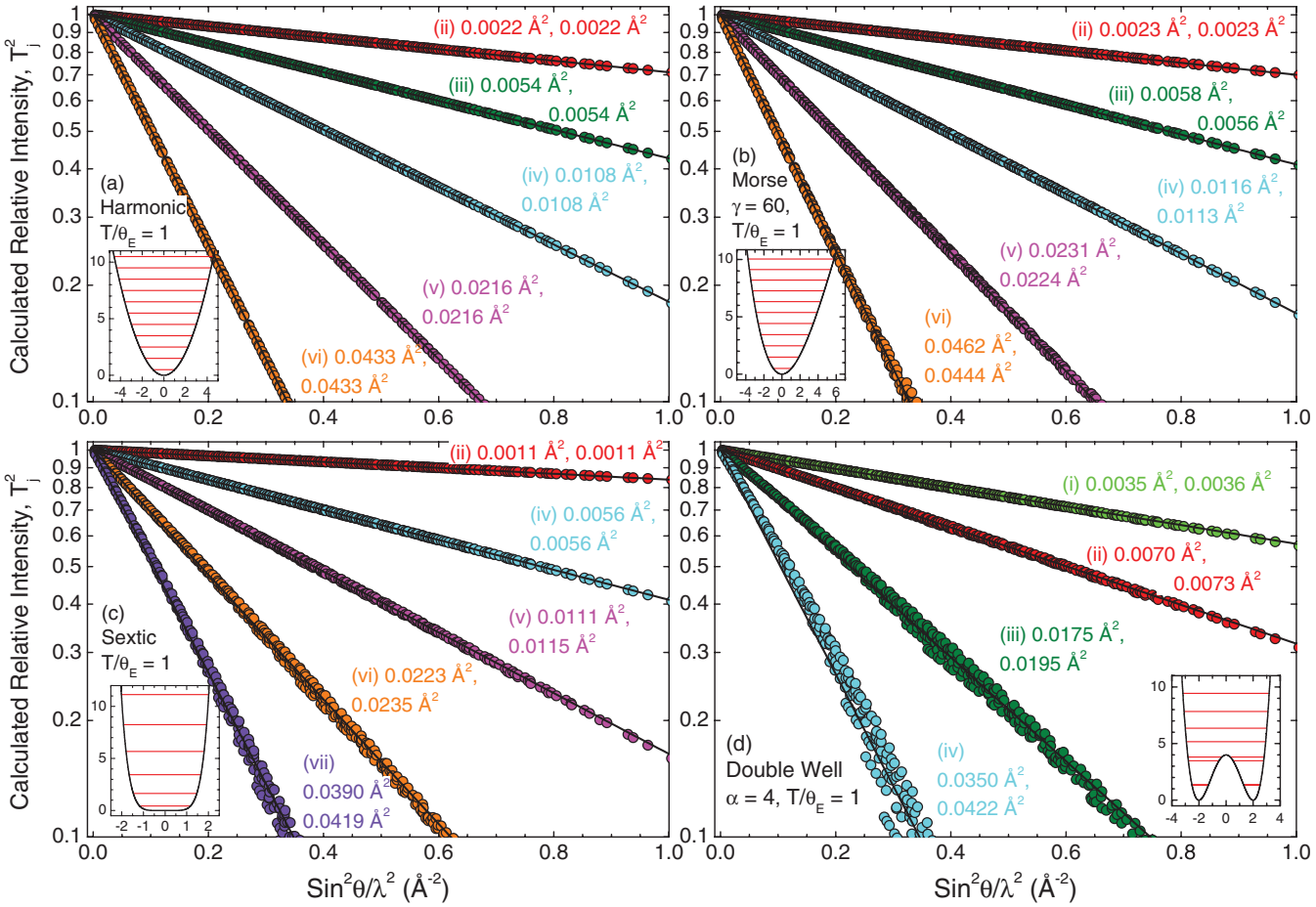

FIG. 1. (Color online) Main panels: Relative intensity T_j^2 vs $\sin^2\theta/\lambda^2$ (Wilson plot) for a crystal whose atoms all vibrate in (a) harmonic, (b) Morse, (c) sextic, and (d) 2–4 double-well potentials. The data points were calculated numerically as described in Sec. III. The lines through the points are fits of the harmonic model for T_j^2. Each set of points and the corresponding fitted line is labeled with a Roman numeral plus two numbers, which denote the values of $\hbar^2/(m_e k_B \theta_E)$, $\langle u^2_{\mathrm{iso},j}\rangle_A$, and $\langle u^2_{\mathrm{iso},j}\rangle_{QH}$ (see text for details). Insets: Schematics of the potentials, with energy eigenstates superimposed. For the double-well potential, the ground state has a small tunnel splitting that is barely visible. In the insets, the ordinate is the energy in units of $\hbar\omega$ ($=k_B\theta_E$), and the abscissa is the displacement in units of $(\hbar^2/(m_e k_B\theta_E))^{1/2}$.

were also done as a function of reduced temperature T/θ_E, or the reduced transformation temperature T/T_c, so that the temperature evolution of $\langle u^2_{\mathrm{iso},j}\rangle_{QH}$ and $\langle u^2_{\mathrm{iso},j}\rangle_A$ could be compared.

IV. ANHARMONIC RATTLING MODES

Figure 1 shows the calculated intensity (T_j^2) versus $\sin^2\theta/\lambda^2$ for crystals whose atoms all vibrate in (a) harmonic, (b) Morse, (c) sextic, and (d) 2–4 double-well potentials. The insets show schematics of the potentials, with the energy eigenstates superimposed. Table I lists their equations. For the Morse potential, we assume a well depth of $\gamma = 60$, which corresponds to the onset of bond dissociation at $T/\theta_E \approx 6$. (Dissociation can be considered as roughly equivalent to melting.) For the double-well potential, we assume a barrier height of $\alpha = 4$ separating the minima. As shown later, this value seems reasonable for rattling modes in particular crystals.

The points in Fig. 1 show the calculated intensities T_j^2 for a reduced temperature of $T/\theta_E = 1$. We have assumed a large lattice parameter, $a = 15$ Å, and a face-centered-cubic structure to provide a high density of (hkl) points in Q space. The maximum value of $\sin^2\theta/\lambda^2 = 1$ corresponds to a Bragg angle of $2\theta = 180°$ for a wavelength of $\lambda = 1$ Å, and $2\theta = 90°$ for $\lambda = 0.71$ Å. The former value of λ corresponds to that for high-resolution neutron diffractometers, whereas the latter is for Mo Kα radiation. The lines through the points are fits of the harmonic model, $T_j^2 = \exp(-16\pi^2\langle u^2_{\mathrm{iso},j}\rangle \sin^2\theta/\lambda^2)$, in the range $0 \leqslant \sin^2\theta/\lambda^2 \leqslant 1$ or $0.1 \leqslant T_j^2 \leqslant 1$. Each set of points and the corresponding fitted line is labeled with a Roman numeral plus two numbers. The numeral denotes the value of $\hbar^2/(m_e k_B\theta_E)$: (i) 0.001, (ii) 0.002, (iii) 0.005, (iv) 0.01, (v) 0.02, (vi) 0.04, and (vii) 0.07 Å^2. The quantity $\hbar^2/(m_e k_B\theta_E)$ is a measure of the zero point $\langle u^2_{\mathrm{iso},j}\rangle$ and provides a convenient way to compare atoms with different masses and characteristic vibrational temperatures. Larger values of $\hbar^2/(m_e k_B\theta_E)$ indicate a smaller effective mass and/or softer interatomic potential. As shown in Fig. 1, anharmonic effects become more pronounced for larger values of $\hbar^2/(m_e k_B\theta_E)$. The values chosen here are representative of vibrations in a wide range of materials, from elemental

U [$\hbar^2/(m_e k_B \theta_E) \approx 0.001$ Å^2] (Ref. 42) to elemental Cs and Na ($\approx$0.01 Å^2) to the anharmonic rattling of the Al guest in VAl_{10} ($\approx$0.07 Å^2).[41] The two numbers following the Roman numeral are $\langle u^2_{\mathrm{iso},j}\rangle_A$, as calculated numerically from quantum statistical mechanics, and $\langle u^2_{\mathrm{iso},j}\rangle_{QH}$, as determined by fitting the harmonic Debye-Waller factor model to the calculated intensity points in the Wilson plot.

As seen in Fig. 1(a), for a harmonic potential the calculated intensity points all fall on straight lines, regardless of the value of $\hbar^2/(m_e k_B \theta_E)$. Moreover, the values of $\langle u^2_{\mathrm{iso},j}\rangle_{QH}$ and $\langle u^2_{\mathrm{iso},j}\rangle_A$ agree perfectly. These results verify the self-consistency of our methods.

For the Morse potential, shown in Fig. 1(b), the points again fall on straight lines, at least for the temperature considered here ($T/\theta_E = 1$). The quasiharmonic values $\langle u^2_{\mathrm{iso},j}\rangle_{QH}$, as deduced from the slopes of the Wilson plots, agree well with the anharmonic values $\langle u^2_{\mathrm{iso},j}\rangle_A$. Even for $\hbar^2/(m_e k_B \theta_E) =$ 0.04 Å^2, the difference is only 4%. Later we show that this conclusion also holds for temperatures much closer to melting.

In the case of a sextic potential, shown in Fig. 1(c), we begin to see more clearly the effects of the anharmonicity. The calculated intensity points begin to show scatter, and there is a slight downward curvature of the Wilson plots. Nonetheless the values of $\langle u^2_{\mathrm{iso},j}\rangle_{QH}$ and $\langle u^2_{\mathrm{iso},j}\rangle_A$ are quite close: for $\hbar^2/(m_e k_B \theta_E) = 0.04$ and 0.07 Å^2, the quasiharmonic values are only $\sim$5% and $\sim$7% too large, respectively. Considering the strong anharmonicity of the sextic potential, and the large values of $\hbar^2/(m_e k_B \theta_E)$, this small error is remarkable. For smaller values of $\hbar^2/(m_e k_B \theta_E)$, there is virtually no difference between $\langle u^2_{\mathrm{iso},j}\rangle_{QH}$ and $\langle u^2_{\mathrm{iso},j}\rangle_A$.

The situation is much the same for the double-well potential. The scatter is significant and the downward curvature clear, particularly for $\hbar^2/(m_e k_B \theta_E) = 0.01$ Å^2. Yet even for this case, the harmonic model fits the data fairly well, and the quasiharmonic value $\langle u^2_{\mathrm{iso},j}\rangle_{QH} = 0.0422$ Å^2 is only $\sim$21% larger than the $\langle u^2_{\mathrm{iso},j}\rangle_A$ value. We should note that we analyzed the double-well potential in exactly the same way as the harmonic, Morse, and sextic potentials. Specifically, we determined the values of both $\langle u^2_{\mathrm{iso},j}\rangle_{QH}$ and $\langle u^2_{\mathrm{iso},j}\rangle_A$ using a single-site model, where the equilibrium atomic position is assumed to be $\langle u_j\rangle = 0$ with respect to the coordinates shown in the Fig. 1 insets. Another approach would be to use a split-site model to account for the multiple minima. Here we chose the single-site model because this is the only option in most Rietveld refinement packages.

The scatter in the calculated intensity points, as seen in Figs. 1(b)–1(d), arises from the anharmonicity of the vibrations. To understand why it is present, one must consider that after evaluation of the scalar product $\vec{Q}\cdot\vec{u}_j$ and expansion of the exponents, the terms of Eq. (2) contain products of the type $k^4\langle u^4_{\mathrm{iso},j}\rangle$, $h^2k^4l^4\langle u^2_{\mathrm{iso},j}\rangle\langle u^4_{\mathrm{iso},j}\rangle^2$, etc. For *anharmonic* potentials, these terms cannot be expressed as factors of $(h^2+k^2+l^2)^n$, where n is an integer. The result is that (hkl) sets which give the same value for $\sin^2\theta/\lambda^2 = (1/4a^2)(h^2 + k^2 + l^2)$ can give *different* values for the calculated intensity. The scatter that we observe in these calculated intensity points should also appear in measured intensity data. However, it might be difficult to distinguish this anharmonicity-caused scatter from the usual scatter in experimental data.

For *harmonic* potentials, the terms of the series can be simplified using $\langle u^4_{\mathrm{iso},j}\rangle = 3\langle u^2_{\mathrm{iso},j}\rangle^2$, $\langle u^6_{\mathrm{iso},j}\rangle = 15\langle u^2_{\mathrm{iso},j}\rangle^3$, $\langle u^8_{\mathrm{iso},j}\rangle = 105\langle u^2_{\mathrm{iso},j}\rangle^4$, etc.[43] By making these substitutions, we find that each term of the series can be written as a factor of $(h^2+k^2+l^2)^n$. As a consequence, any (hkl) set that gives a particular value for $\sin^2\theta/\lambda^2$ also gives the same intensity, and there is no scatter in the calculated harmonic points.

Figure 2 shows the temperature dependence of $\langle u^2_{\mathrm{iso},j}\rangle$, plotted in nondimensional form as $\langle u^2_{\mathrm{iso},j}\rangle m_e k_B \theta_E/\hbar^2$ versus T/θ_E, for the same single-particle potentials as in Fig. 1. The points show values of $\langle u^2_{\mathrm{iso},j}\rangle_{QH}$ determined from slopes of Wilson plots, whereas the curves show values of $\langle u^2_{\mathrm{iso},j}\rangle_A$ computed using quantum statistical mechanics. For each type of potential, there is one curve for $\langle u^2_{\mathrm{iso},j}\rangle_A$, regardless of the value of $\hbar^2/(m_e k_B \theta_E)$, because of the normalization of the ordinate. For the harmonic vibration, shown in Fig. 2(a), the curve and points agree exactly for all temperatures and values of $\hbar^2/(m_e k_B \theta_E)$, as we expect. For each anharmonic vibration, the points deviate from the curve, and the deviation grows as the value of $\hbar^2/(m_e k_B \theta_E)$ increases. The differences between the curves and the points, and between the points for different values of $\hbar^2/(m_e k_B \theta_E)$, are due to fitting of the anharmonic calculated intensities with the harmonic Debye-Waller model. Specifically, the harmonic model cannot account for the scatter and curvature that is present in the Wilson plots.

We should comment briefly on the temperature dependence of $\langle u^2_{\mathrm{iso},j}\rangle$ for the anharmonic vibrations. Notice that for the Morse potential, shown in Fig. 2(b), $\langle u^2_{\mathrm{iso},j}\rangle$ increases with temperature more rapidly than for a harmonic potential. This behavior is expected for "high-temperature" anharmonicity, where with increasing vibrational energy (temperature) the Morse potential widens more rapidly than the harmonic potential. This can be seen in the Fig. 1 insets, where the ordinates and abscissas are normalized to account for different values of m_e and θ_E. For the sextic vibration, $\langle u^2_{\mathrm{iso},j}\rangle$ increases more slowly with temperature than for the harmonic vibration. The reason is that the sextic potential is steep walled and boxlike, which restricts the atomic displacements compared to the harmonic potential. This is especially true for higher energies (temperatures), where the value of $\langle u^2_{\mathrm{iso},j}\rangle$ seems to saturate.

The most interesting temperature dependence belongs to the double-well potential. At low temperatures, the atom resides mainly in the split portion of the double well [see Fig. 1(d) inset]. Because these split lobes have large static displacement relative to $u = 0$, the value of $\langle u^2_{\mathrm{iso},j}\rangle$ is large at low temperatures. The value of $\langle u^2_{\mathrm{iso},j}\rangle$ remains approximately constant in the range $0 < T/\theta_E < 0.5$, due to confinement to the split region. For $T/\theta_E > 0.5$, the atom can populate vibrational states above the split, where there is a higher probability of being found close to $u = 0$. Initially this leads to a decrease in $\langle u^2_{\mathrm{iso},j}\rangle$ in the range $0.5 < T/\theta_E < 2.5$. For even higher temperatures, $T/\theta_E > 2.5$, the increasing population of states above the split causes $\langle u^2_{\mathrm{iso},j}\rangle$ to reach a minimum and eventually increase with temperature in a more usual way.

The insets of Fig. 2 show the temperature dependence of $\Delta\langle u^2_{\mathrm{iso},j}\rangle/\langle u^2_{\mathrm{iso},j}\rangle_A$, where $\Delta\langle u^2_{\mathrm{iso},j}\rangle = \langle u^2_{\mathrm{iso},j}\rangle_{QH} - \langle u^2_{\mathrm{iso},j}\rangle_A$

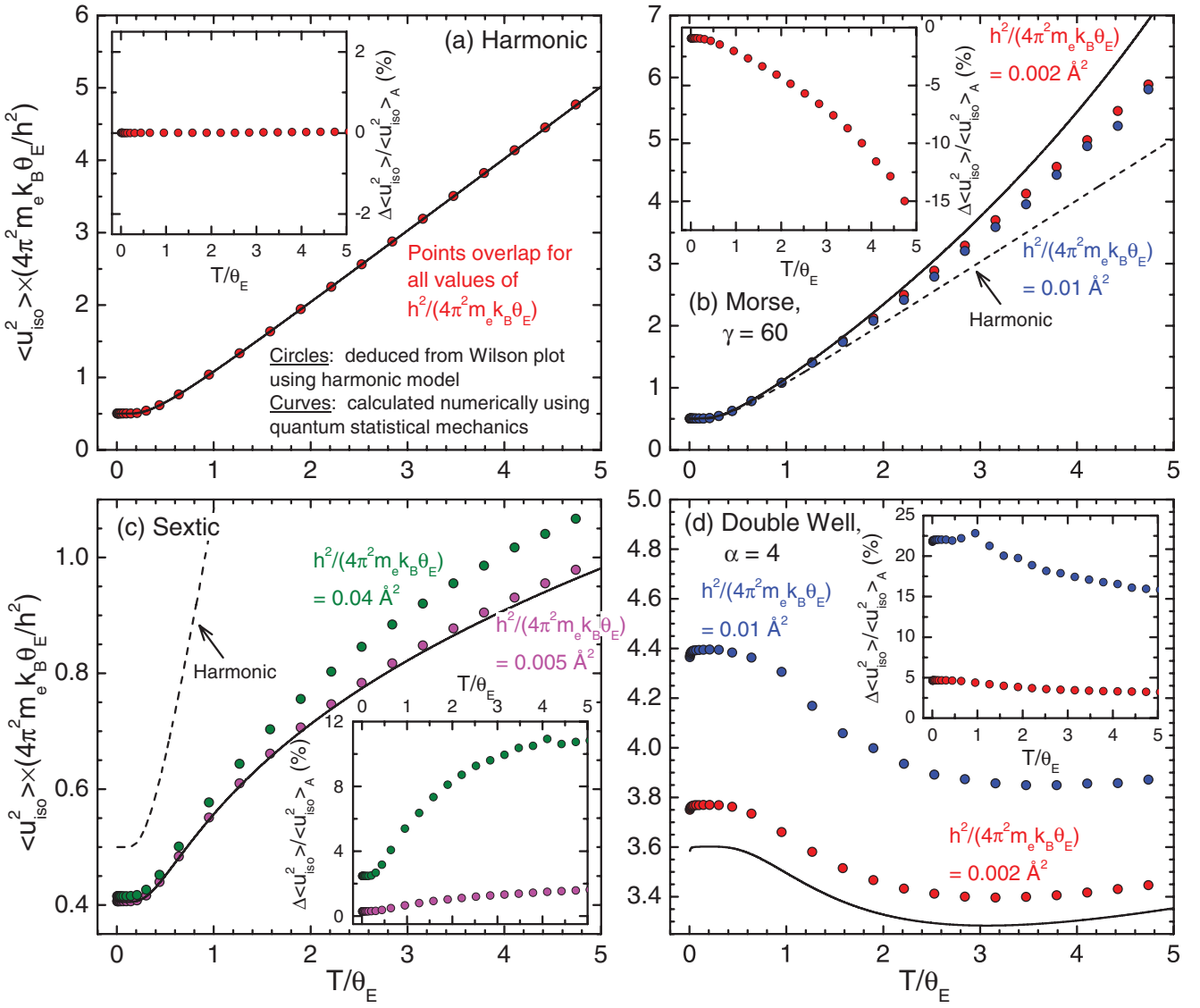

FIG. 2. (Color online) Temperature dependence of $\langle u^2_{\mathrm{iso},j}\rangle$, plotted as $\langle u^2_{\mathrm{iso},j}\rangle m_e k_B \theta_E/\hbar^2$ vs T/θ_E, for a crystal whose atoms all vibrate in (a) harmonic, (b) Morse, (c) sextic, and (d) 2–4 double-well potentials. The points denote quasiharmonic values $\langle u^2_{\mathrm{iso},j}\rangle_{QH}$ that were determined by fitting the harmonic Debye-Waller model to the calculated intensities, as done in Fig. 1. The curves denote anharmonic values $\langle u^2_{\mathrm{iso},j}\rangle_A$ that were computed numerically using quantum statistical mechanics. Inset figures show the temperature dependence of the relative error $\Delta\langle u^2_{\mathrm{iso},j}\rangle/\langle u^2_{\mathrm{iso},j}\rangle_A$ for different values of $\hbar^2/(m_e k_B \theta_E)$. The scatter in $\Delta\langle u^2_{\mathrm{iso},j}\rangle/\langle u^2_{\mathrm{iso},j}\rangle_A$, evident for the sextic and double-well potentials, is an artifact of the scatter in the Wilson plots.

is the error associated with the harmonic analysis of the anharmonic data. As expected, the error is zero for the harmonic vibration, but increases as the anharmonicity grows. Nonetheless, the largest error is only ∼23%, which we find for the 2–4 double-well potential at low temperatures. Notice that even for the strong anharmonicity considered here, the temperature dependence of $\langle u^2_{\mathrm{iso},j}\rangle_{QH}$ follows that of $\langle u^2_{\mathrm{iso},j}\rangle_A$.

V. ANHARMONIC VIBRATIONS NEAR SECOND-ORDER PHASE TRANSITIONS

Near a second-order structural phase transition, the temperature dependence of the Gibbs free energy can be approximated using a 2–4 Landau potential,[44]

$$G(T) = G_0 + \tfrac{1}{2}a(T - T_c)u^2 + \tfrac{1}{4}Bu^4, \qquad (3)$$

where G_0 is the free energy of the high-symmetry phase (in the absence of vibrations), T_c is the phase-transition temperature, and a and B are coefficients of the harmonic and quartic terms. Here we assume that all parameters are temperature independent. Within the Landau framework, the transition is modeled using a single-particle potential, with a temperature-dependent harmonic term to account for the long-range elastic interactions that are associated with the transformation. In Eq. (3), we have already assumed that the order parameter η corresponds to the average displacement $\langle u\rangle$ for atoms or groups of atoms located at particular Wyckoff sites. This is a standard assumption for displacive-type transformations.[43]

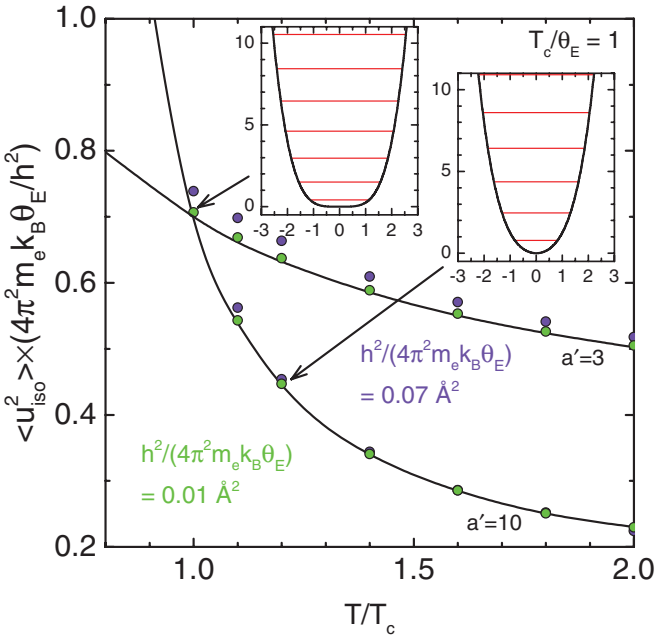

FIG. 3. (Color online) Temperature dependence of $\langle u^2_{\mathrm{iso},j}\rangle$ in the vicinity of a second-order displacive transition, plotted as $\langle u^2_{\mathrm{iso},j}\rangle m_e k_B\theta_E/\hbar^2$ vs T/T_c. The effective single-site potential is modeled using a 2–4 Landau potential with $T_c/\theta_E = 1$ and $a' = 3$ and 10 (see Table I). The curves show values of $\langle u^2_{\mathrm{iso},j}\rangle_A$, whereas the points show values of $\langle u^2_{\mathrm{iso},j}\rangle_{QH}$ for $\hbar^2/m_e k_B\theta_E = 0.01$ Å^2 and 0.07 Å^2. Notice that for $a' = 10$, some of the 0.01 and 0.07 Å^2 points overlap. The insets are schematics of the 2–4 Landau potential for $T/T_c = 1$ and $T/T_c = 1.2$ ($a' = 10$). In the insets, the ordinate is the energy in units of $\hbar\omega$ ($= k_B\theta_E$), and the abscissa is the displacement in units of $(\hbar^2/(m_e k_B\theta_E))^{1/2}$.

In this case, Eq. (3) is equivalent to a single-site potential for the atoms undergoing displacement. Then by analogy with the 2–4 double well (see Table I), we can rewrite Eq. (3) as

$$G(T) = G_0 + \frac{1}{2}a'\frac{T-T_c}{\theta_E}\left(\frac{k_B\theta_E m_e}{\hbar^2}\right)k_B\theta_E u^2 + \frac{1}{4}\left(\frac{k_B\theta_E m_e}{\hbar^2}\right)^2 k_B\theta_E u^4, \quad (4)$$

where a' is a constant and the other parameters have already been defined.

Figure 3 shows the temperature dependence of $\langle u^2_{\mathrm{iso},j}\rangle$ for the single-particle potential of Eq. (4), plotted nondimensionally as $\langle u^2_{\mathrm{iso},j}\rangle m_e k_B\theta_E/\hbar^2$ vs T/T_c. Here we show results for a relative transition temperature of $T_c/\theta_E = 1$ and harmonic term coefficients of $a' = 3$ and 10. For both values of a', we performed calculations assuming $\hbar^2/m_e k_B\theta_E = 0.01$ Å^2 and $\hbar^2/m_e k_B\theta_E = 0.07$ Å^2. The latter case represents a particularly small effective mass and/or soft interatomic potential, where anharmonic effects should be most evident. It is important to note that we obtained results comparable to those shown in Fig. 3 by using a wide range of T_c/θ_E, a', and $\hbar^2/m_e k_B\theta_E$ values.

The curves in Fig. 3 show anharmonic values $\langle u^2_{\mathrm{iso},j}\rangle_A$, whereas the points show quasiharmonic values $\langle u^2_{\mathrm{iso},j}\rangle_{QH}$. For particular values of T_c/θ_E and a', there is one curve for $\langle u^2_{\mathrm{iso},j}\rangle_A$ regardless of the value of $\hbar^2/m_e k_B\theta_E$. As seen in the figure, $\langle u^2_{\mathrm{iso},j}\rangle$ increases as the temperature decreases toward $T = T_c$. The reason is that the harmonic contribution to the potential becomes softer, and hence the potential well becomes progressively wider, until at $T = T_c$ the harmonic term disappears and the potential is purely quartic. This trend is seen in the Fig. 3 insets. Despite the increased anharmonicity at lower temperatures, the values of $\langle u^2_{\mathrm{iso},j}\rangle_{QH}$ and $\langle u^2_{\mathrm{iso},j}\rangle_A$ agree closely. Even for $\hbar^2/m_e k_B\theta_E = 0.07$ Å^2, the relative error $\Delta\langle u^2_{\mathrm{iso},j}\rangle/\langle u^2_{\mathrm{iso},j}\rangle_A$ is only 6% at $T/T_c = 1$. The small error is not surprising, given that the Landau potential has similar anharmonicity to the sextic and double-well potentials considered in Sec. IV. Based on this analysis, together with the rattling-mode analyses in the previous section, we can safely assume that $\langle u^2_{\mathrm{iso},j}\rangle_{QH} \approx \langle u^2_{\mathrm{iso},j}\rangle_A$ in the vicinity of most phase transitions.

Below T_c, the crystal distorts from the high-symmetry structure into a lower-symmetry one. For these temperatures, it is perhaps more correct to measure $\langle u^2_{\mathrm{iso},j}\rangle$ relative to the new Wyckoff sites of the low-symmetry (distorted) phase. If we instead continue to describe the atomic position in terms of the high-symmetry phase, then the values of $\langle u^2_{\mathrm{iso},j}\rangle$ will continue to increase as the temperature decreases below T_c. This result is shown in Fig. 3. In this case, there are two contributions to $\langle u^2_{\mathrm{iso},j}\rangle$: one associated with the static atomic displacements (e.g., movement of the equilibrium atomic position away from $\langle u_j\rangle = 0$), and one associated with the dynamic displacements of the vibration.

VI. COMPARISON WITH EXPERIMENTAL DATA

In the preceding sections, we showed that the MSAD for an anharmonic vibration, $\langle u^2_{\mathrm{iso},j}\rangle_A$, is well approximated using the quasiharmonic value, $\langle u^2_{\mathrm{iso},j}\rangle_{QH}$. To demonstrate this, we assumed various single-particle anharmonic potentials and calculated $\langle u^2_{\mathrm{iso},j}\rangle_A$ and $\langle u^2_{\mathrm{iso},j}\rangle_{QH}$ for each model. In this section, we present $\langle u^2_{\mathrm{iso},j}\rangle$ versus temperature data for a particular atom in two different crystals. These data suggest that both atoms vibrate with strong anharmonicity. Moreover, we show that one atom is well described using a sextic anharmonic model, whereas the other is described using a double-well model.

Figure 4 shows the temperature dependence of $\langle u^2_{\mathrm{iso},j}\rangle$ for the Al guest atom in $VAl_{10.1}$, and for the Eu guest in $Eu_8Ga_{16}Ge_{30}$. The data for $VAl_{10.1}$ are our own,[41] whereas the data for $Eu_8Ga_{16}Ge_{30}$ were obtained from Ref. 4. For both materials, the values of $\langle u^2_{\mathrm{iso},j}\rangle$ were determined via Rietveld refinement of neutron-diffraction data, using a single-site crystallographic model for the guest atom and the harmonic and isotropic model for the temperature factor. In terms of the notation defined in this paper, these MSAD values are quasiharmonic, $\langle u^2_{\mathrm{iso},j}\rangle_{QH}$.

The structures of both $VAl_{10.1}$ and $Eu_8Ga_{16}Ge_{30}$ are characterized by a network of polyhedral cages, each of which can accommodate one guest atom.[4,41] The cages are oversized compared to the guests, and the guests undergo low frequency ($\hbar\omega \sim 2$–5 meV) and large amplitude vibrations that are often described as "rattling." Studies have suggested that many, but

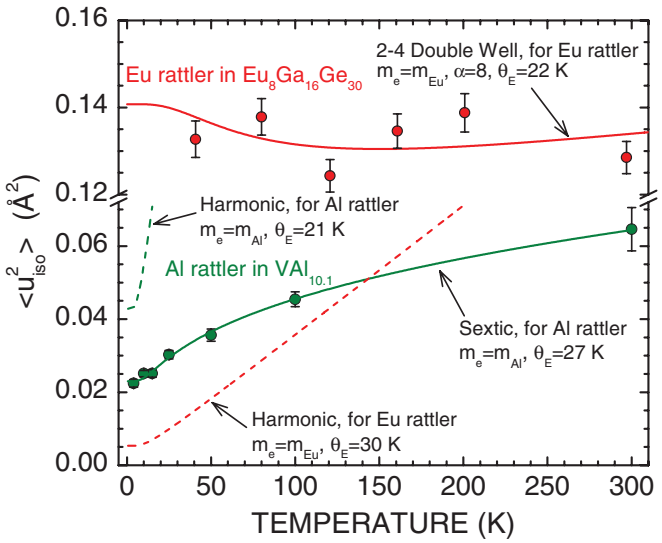

FIG. 4. (Color online) Temperature dependence of $\langle u^2_{\mathrm{iso},j}\rangle$ for the Eu rattling atom in $Eu_8Ga_{16}Ge_{30}$ and the Al rattling atom in $VAl_{10.1}$. The data points are experimental values of $\langle u^2_{\mathrm{iso},j}\rangle_{QH}$ obtained from Refs. 4 and 41. The dashed curves were calculated using the harmonic oscillator model for the indicated values of m_e and θ_E, whereas the solid curves were computed using sextic and 2–4 double-well models for the indicated parameter values. Note the break in the ordinate axis.

not all, rattling modes have strong anharmonicity.[4,11,41,45–48] To investigate the anharmonicity of the guest vibrations in $VAl_{10.1}$ and $Eu_8Ga_{16}Ge_{30}$, we first calculated the expected temperature dependence of $\langle u^2_{\mathrm{iso},j}\rangle$ assuming that the rattling is harmonic and dispersionless. The results of these calculations are shown by the dashed curves in Fig. 4. Here we used the free-atom masses together with the literature values of $\theta_E = 21$ K for $VAl_{10.1}$ and $\theta_E = 30$ K for $Eu_8Ga_{16}Ge_{30}$, which were determined from low-temperature heat-capacity measurements.[4,41] As seen in Fig. 4, the harmonic model cannot reproduce the temperature dependence of $\langle u^2_{\mathrm{iso},j}\rangle$ for the rattling atoms.

The solid curves in Fig. 4 show the temperature dependence of $\langle u^2_{\mathrm{iso},j}\rangle_A$, calculated using a sextic potential with $m = m_{Al}$ and $\theta_E = 27$ K for the Al rattler, and using a 2–4 double-well potential with $m = m_{Eu}$, $\theta_E = 22$ K, and $\alpha = 8$ for the Eu rattler. For these calculations, we included a temperature-independent term $\langle u^2_{\mathrm{iso},j}\rangle_0$, so that $\langle u^2_{\mathrm{iso},j}\rangle_A = \langle u^2_{\mathrm{iso},j}\rangle_0 + \sum_n p_n \langle \Psi_n|u^2|\Psi_n\rangle$. This term accounts for systematic errors in the experimental data and Rietveld refinement.[42] As shown in the figure, the data for the Al rattler are well described by the calculated curve. For the Eu rattler, the scatter in the data and the larger error bars tend to blur the details of the temperature dependence. Nonetheless, we can see that the data are generally independent of temperature, and this behavior is reproduced by the double-well model. Our assumption of a multiple-well potential for Eu is supported by nuclear density maps developed from single-crystal neutron diffraction,[4] and by Mossbauer and microwave absorption experiments.[49] The maps indicate that for temperatures near 40 K, the Eu nuclear density splits into four crystallographically equivalent sites, each displaced symmetrically from the original site by about ~0.4 Å. The Mossbauer and microwave measurements show direct experimental evidence for Eu tunneling between the four sites.

The agreement between our calculations and experimental data supports our conclusion in Secs. IV and V, namely, that the harmonic temperature factor can virtually always be used to deduce reliable thermal parameters, even for the case of strong anharmonicity. Furthermore, it suggests that anharmonic potentials similar to those assumed in Sec. IV do occur in nature. We should recognize, however, that these simple potentials are probably only rough approximations for the true rattling atom potentials. Most likely, the good agreement between the data and the curves points to the insensitivity of $\langle u^2_{\mathrm{iso},j}\rangle$ to the details of the potentials.

With regard to phase transitions, it is well known from experiment that $\langle u^2_{\mathrm{iso},j}\rangle$ for the displacing atom(s) usually increases as temperature decreases toward T_c. The observed behavior is usually similar to that shown in Fig. 4. This temperature dependence was the subject of numerous experimental and theoretical studies during the 1970s and 1980s.[20,21,23,50,51] We will not discuss these data here. Based on the analyses presented in Secs. V and IV, we can safely conclude that $\langle u^2_{\mathrm{iso},j}\rangle_{QH}$ and $\langle u^2_{\mathrm{iso},j}\rangle_A$ are nearly equal in the vicinity of a phase transformation.

VII. SUMMARY AND CONCLUSIONS

In the structural refinement of diffraction data, one normally uses the harmonic temperature factor, e.g., $T_j = \exp(-8\pi^2\langle u^2_{\mathrm{iso},j}\rangle \sin^2\theta/\lambda^2)$, to deduce values for the mean-square atomic displacements $\langle u^2_{\mathrm{iso},j}\rangle$. For most materials, as well as temperature, pressure, and field conditions, the phonons have small anharmonicity, so use of the harmonic model is justified. For some materials and conditions, however, particular atoms may vibrate with strong anharmonicity. In this case, we expect the harmonic model to give erroneous values of $\langle u^2_{\mathrm{iso},j}\rangle$. Examples include "rattling atoms" in particular crystal structures,[4,11,18,41] atoms that are displaced in the vicinity of a continuous phase transition,[20,21,23,50,51] and atoms in a crystal that is close to its melting point.[30] For these cases, a rigorously correct analysis requires an anharmonic expression for T_j that is based on statistics or on a single-particle model of the anharmonic vibration.

Our present results show that the value and temperature dependence of $\langle u^2_{\mathrm{iso},j}\rangle$ can be determined accurately by analyzing diffraction data in terms of the *harmonic* temperature (Debye-Waller) factor, regardless of the anharmonicity of the vibration. We demonstrated this by calculating Bragg intensities for various anharmonic model crystals, and then analyzing these calculated intensities in terms of the harmonic Debye-Waller factor to deduce quasiharmonic values $\langle u^2_{\mathrm{iso},j}\rangle_{QH}$. These values were then compared to the anharmonic values $\langle u^2_{\mathrm{iso},j}\rangle_A$ that we calculated using quantum statistical mechanics. We found that even for strongly anharmonic potentials and for extreme low and high temperatures, the quasiharmonic values are in error by at most 25%. Moreover, the temperature dependences of $\langle u^2_{\mathrm{iso},j}\rangle_{QH}$ and $\langle u^2_{\mathrm{iso},j}\rangle_A$ track closely. This latter result is especially relevant to the interpretation of temperature-dependent phenomena. It is important to stress

that for these analyses, we used model anharmonic crystals that represented a worst-case scenario where *every* site in the structure was characterized by large vibrational anharmonicity. For real crystals, where only a small fraction of sites have strong anharmonicity, we expect the errors to be even smaller.

ACKNOWLEDGMENTS

The authors thank A. C. Lawson, D. C. Wallace, and E. K. H. Salje for discussions and critiques of the manuscript. This work was funded in part by the LANL Laboratory Directed Research and Development program.

[1] H. J. Lipkin, e-print arXiv:cond-mat/0405023.

[2] B. T. M. Willis and A. W. Pryor, *Thermal Vibrations in Crystallography* (Cambridge University Press, Cambridge, UK, 1975).

[3] A. C. Larson and R. B. Von Dreele, *General Structure Analysis System (GSAS)*, Los Alamos National Laboratory Technology Report No. LAUR 86-748, 2004 (unpublished).

[4] B. C. Sales, B. C. Chakoumakos, R. Jin, J. R. Thompson, and D. Mandrus, Phys. Rev. B **63**, 245113 (2001).

[5] S. Paschen, V. H. Tran, M. Baenitz, W. Carrillo-Cabrera, Y. Grin, and F. Steglich, Phys. Rev. B **65**, 134435 (2002).

[6] J. S. Tse, V. P. Shpakov, V. V. Murashov, and V. R. Belosludov, J. Chem. Phys. **107**, 9271 (1997).

[7] M. Christensen, A. B. Abrahamsen, N. B. Christensen, F. Juranyi, N. H. Andersen, K. Lefmann, J. Andreasson, C. R. H. Bahl, and B. B. Iversen, Nature Mater. **7**, 811 (2008).

[8] M. M. Koza, M. R. Johnson, R. Viennois, H. Mutka, L. Girard, and D. Ravot, Nature Mater. **7**, 805 (2008).

[9] A. D. Caplin, G. Grüner, and J. B. Dunlop, Phys. Rev. Lett. **30**, 1138 (1973).

[10] J. I. Yamaura, S. Yonezawa, Y. Muraoka, and Z. Hiroi, J. Solid State Chem. **179**, 336 (2006).

[11] T. Dahm and K. Ueda, Phys. Rev. Lett. **99**, 187003 (2007).

[12] T. Mori, K. Iwamoto, S. Kushibiki, H. Honda, H. Matsumoto, N. Toyota, M. A. Avila, K. Suekuni, and T. Takabatake, Phys. Rev. Lett. **106**, 015501 (2011).

[13] F. M. Grosche, H. Q. Yuan, W. Carrillo-Cabrera, S. Paschen, C. Langhammer, F. Kromer, G. Sparn, M. Baenitz, Y. Grin, and F. Steglich, Phys. Rev. Lett. **87**, 247003 (2001).

[14] Y. Nagao, J. I. Yamaura, H. Ogusu, Y. Okamoto, and Z. Hiroi, J. Phys. Soc. Jpn. **78**, 064702 (2009).

[15] E. D. Bauer, N. A. Frederick, P.-C. Ho, V. S. Zapf, and M. B. Maple, Phys. Rev. B **65**, 100506 (2002).

[16] S. Sanada, Y. Aoki, H. Aoki, A. Tsuchiya, D. Kikuchi, H. Sugawara, and H. Sato, J. Phys. Soc. Jpn. **74**, 246 (2005).

[17] B. C. Sales, D. Mandrus, B. C. Chakoumakos, V. Keppens, and J. R. Thompson, Phys. Rev. B **56**, 15081 (1997).

[18] B. C. Sales, B. C. Chakoumakos, and D. Mandrus, Phys. Rev. B **61**, 2475 (2000).

[19] G. A. Samara and B. Morosin, Phys. Rev. B **8**, 1256 (1973).

[20] J. A. Zvirgzds and J. V. Zvirgzde, Phys. Status Solidi B **101**, K21 (1980).

[21] P. Kapostinš, I. Zitars, and J. Zvirgzds, Ferroelectrics **79**, 185 (1988).

[22] N. N. Sirota and L. P. Polutchankina, Kristall und Technik **16**, 1145 (1981).

[23] M. Sakata, J. Harada, M. J. Cooper, and K. D. Rouse, Acta Crystallogr. Sect. A **36**, 7 (1980).

[24] J. F. Scott, Rev. Mod. Phys. **46**, 83 (1974).

[25] J. C. Lashley, S. M. Shapiro, B. L. Winn, C. P. Opeil, M. E. Manley, A. Alatas, W. Ratcliff, T. Park, R. A. Fisher, B. Mihaila, P. Riseborough, E. K. H. Salje, and J. L. Smith, Phys. Rev. Lett. **101**, 135703 (2008).

[26] C. K. Johnson, Acta Crystallogr. Sect. A **25**, 187 (1969).

[27] U. H. Zucker and H. Schulz, Acta Crystallogr. Sect. A **38**, 563 (1982).

[28] U. H. Zucker and H. Schulz, Acta Crystallogr. Sect. A **38**, 568 (1982).

[29] W. F. Kuhs, Acta Crystallogr. Sect. A **48**, 80 (1992).

[30] A. A. Maradudin and P. A. Flinn, Phys. Rev. **129**, 2529 (1963).

[31] B. Dawson and B. T. M. Willis, Proc. R. Soc. London A **298**, 307 (1967).

[32] J. G. Dash, D. P. Johnson, and W. M. Visscher, Phys. Rev. **168**, 1087 (1968).

[33] B. T. M. Willis, Acta Crystallogr. Sect. A **25**, 277 (1969).

[34] K. Tanaka and F. Marumo, Acta Crystallogr. Sect. A **39**, 631 (1983).

[35] C. Scheringer, Acta Crystallogr. Sect. A **41**, 73 (1985).

[36] K. N. Trueblood, H.-B. Bürgi, H. Burzlaff, J. D. Dunitz, C. M. Gramaccioli, H. H. Schulz, U. Shmueli, and S. C. Abrahams, Acta Crystallogr. Sect. A **52**, 770 (1996).

[37] C. Kittel, *Introduction to Solid State Physics*, 7th ed. (Wiley, New York, 1996).

[38] B. E. Warren, *X-Ray Diffraction* (Addison-Wesley, Reading, MA, 1969).

[39] S. W. Lovesey, *Theory of Neutron Scattering from Condensed Matter*, International Series of Monographs on Physics, Vol. 1 (Clarendon, Oxford, 1984).

[40] M. K. Transtrum, B. B. Machta, and J. P. Sethna, Phys. Rev. Lett. **104**, 060201 (2010).

[41] D. J. Safarik, T. Klimczuk, A. Llobet, D. D. Byler, J. C. Lashley, J. R. O'Brien, and N. R. Dilley, Phys. Rev. B **85**, 014103 (2012).

[42] A. Lawson, J. Goldstone, B. Cort, R. Sheldon, and E. Foltyn, J. Alloys Compd. **213-214**, 426 (1994).

[43] E. K. H. Salje, B. Wruck, and H. Thomas, Z. Phys. B **82**, 399 (1991).

[44] E. K. H. Salje, *Phase Transitions in Ferroelastic and Co-elastic Crystals* (Cambridge University Press, Cambridge, UK, 1990).

[45] A. Bentien, B. B. Iversen, J. D. Bryan, G. D. Stucky, A. E. C. Palmqvist, A. J. Schultz, and R. W. Henning, J. Appl. Phys. **91**, 5694 (2002).

[46] L. Qiu, I. P. Swainson, G. S. Nolas, and M. A. White, Phys. Rev. B **70**, 035208 (2004).

[47] T. Mori, S. Goshima, K. Iwamoto, S. Kushibiki, H. Matsumoto, N. Toyota, K. Suekuni, M. A. Avila, T. Takabatake, T. Hasegawa, N. Ogita, and M. Udagawa, Phys. Rev. B **79**, 212301 (2009).

[48] H. Matsumoto, T. Mori, K. Iwamoto, S. Goshima, S. Kushibiki, and N. Toyota, Phys. Rev. B **79**, 214306 (2009).

[49] R. P. Hermann, V. Keppens, P. Bonville, G. S. Nolas, F. Grandjean, G. J. Long, H. M. Christen, B. C. Chakoumakos, B. C. Sales, and D. Mandrus, Phys. Rev. Lett. **97**, 017401 (2006).

[50] G. M. Meyer and R. A. Cowley, Ferroelectrics **11**, 479 (1976).

[51] S. L. Mair, Phys. Rev. B **28**, 2866 (1983).